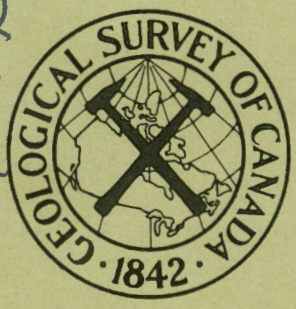

GEOLOGICAL SURVEY OF CANADA

DEPARTMENT OF ENERGY, MINES AND RESOURCES

PAPER 68-32

THE FERRO-MANGANESE PAVEMENT ON SAN PABLO SEAMOUNT

(Report and 10 figures)

F. Aumento, D. E. Lawrence, and A. G. Plant

GEOLOGICAL SURVEY
OF CANADA

PAPER 68-32

THE FERRO-MANGANESE PAVEMENT ON SAN PABLO SEAMOUNT

F. Aumento, D. E. Lawrence, and A. G. Plant

DEPARTMENT OF ENERGY, MINES AND RESOURCES

Available by mail from the Queen's Printer, Ottawa,

from Geological Survey of Canada,
601 Booth St., Ottawa,

and at the following Canadian Government bookshops:

HALIFAX
1735 Barrington Street

MONTREAL
Æterna-Vie Building, 1182 St. Catherine St. West

OTTAWA
Daly Building, Corner Mackenzie and Rideau

TORONTO
221 Yonge Street

WINNIPEG
Mall Center Bldg., 499 Portage Avenue

VANCOUVER
657 Granville Street

or through your bookseller

Price $1.50 Catalogue No. M44-68-32

Price subject to change without notice

ROGER DUHAMEL, F.R.S.C.
Queen's Printer and Controller of Stationery
Ottawa, Canada
1968

CONTENTS

ABSTRACT

A well bedded ferro-manganese pavement overlies the slopes of San Pablo Seamount. Results from chemical, X-ray, electron microscope and electron microprobe analyses of the pavement are compared with data from other known ferro-manganese deposits.

SAN PABLO SEAMOUNT

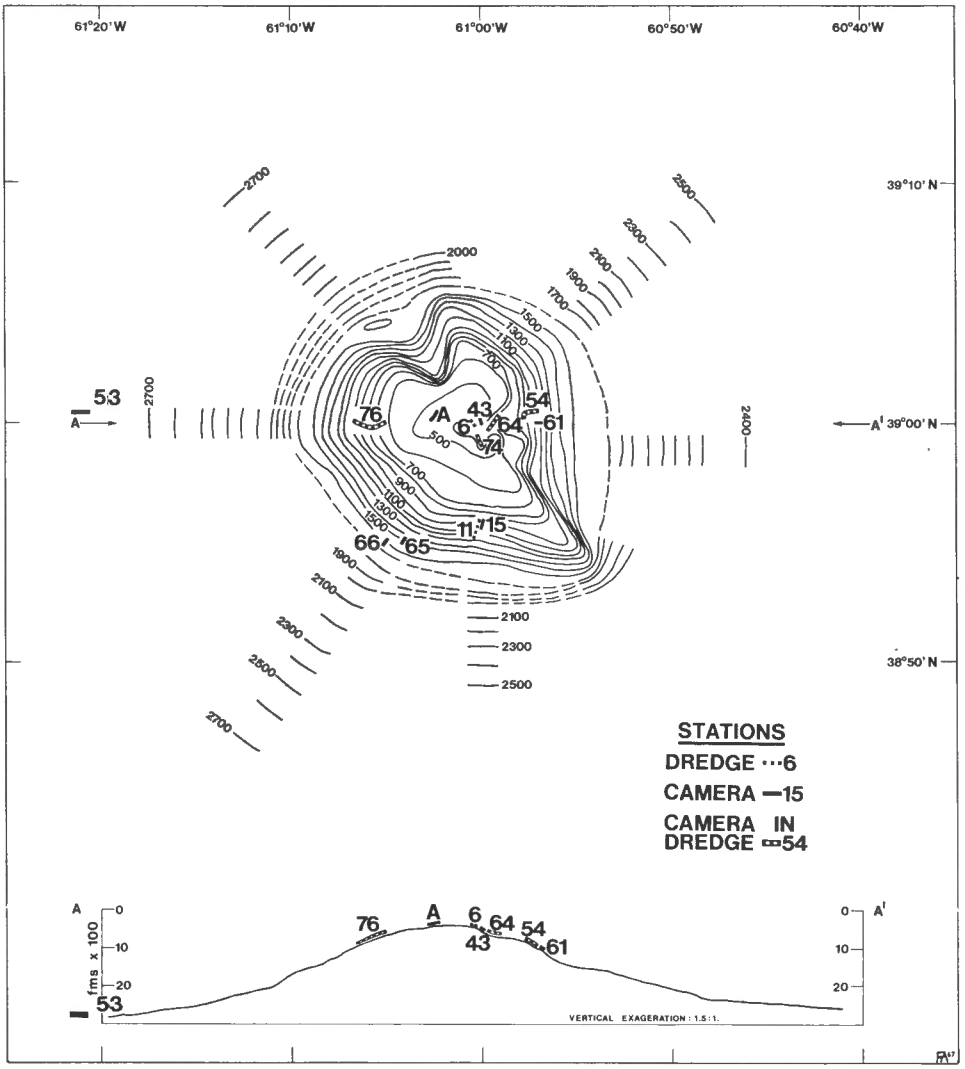

Figure 1 Bathymetry and station locations, San Pablo Seamount. Depths are in fathoms uncorrected for the speed of sound in water.

THE FERRO-MANGANESE PAVEMENT ON SAN PABLO SEAMOUNT

INTRODUCTION

Two of the authors, F. Aumento and D. E. Lawrence, were given the opportunity to sample San Pablo Seamount (39°N, 61°W), one of the Kelvin Seamounts, during the 1967 Bedford Institute of Oceanography Meteorological Cruise (Hudson Cruise 19-67).

A survey of the seamount was begun in 1966 when a number of parallel survey lines were made with the ship navigating relative to a radar transponder buoy moored on top of the seamount. A second set of survey lines was completed in 1967 using a second radar transponder buoy and Loran navigational aid; these survey lines are in a star pattern, providing diminishing detail with increasing distance from the centre of the seamount. A compilation of both surveys is given in Figure 1, where depths are given in fathoms uncorrected for the speed of sound in water.

San Pablo Seamount has the form of a large shield volcano with a terrace at 1, 600 fathoms and a relatively flat top between 700 and 500 fathoms; its shallowest point is about 480 fathoms below sea-level. Its sides are relatively steep between 700 and 2, 000 fathoms but there is a marked change in gradient at about 2, 000 fathoms (the change occurs at slightly different depths on different sides of the seamount). At this point the sides begin to grade into the flat ocean deep which extends to a depth of 2, 900 fathoms. The higher reaches (500-600 fathoms) of the seamount are truncated by a northwest trending linear feature. This feature is parallel to the orientation of the distribution of the other Kelvin Seamounts; it may be a fracture zone on the sea floor which acted as the feeder for the volcanoes forming these seamounts. The feeder, filled with volcanic material more compact than that forming the shield volcano itself, may have withstood the sea's weathering effect better than the extruded material, thus forming a prominent feature on the slopes of San Pablo Seamount.

CAMERA AND DREDGE STATIONS

Bottom photographs taken in 1966 (camera station 'A', Fig. 1) showed what were incorrectly interpreted as extensive beds of weathered lava flows (Fig. 2) covering the top of the seamount. However, it became clear, as soon as dredge station No. 6 was taken in 1967, that these 'lava flows' were in fact thickly bedded ferro-manganese deposits. Successive camera and dredge stations (see Fig. 1) confirmed the existence of these bedded ferro-manganese deposits down to 1, 600 fathoms; piston cores taken at depths

Manuscript received: March 19, 1968.

A

Figure 2 A, B: Bottom photographs of the ferro-manganese pavement on the relatively flat top of San Pablo Seamount. The small, irregular depressions are filled with organic debris and detrital material. The thin white lines on

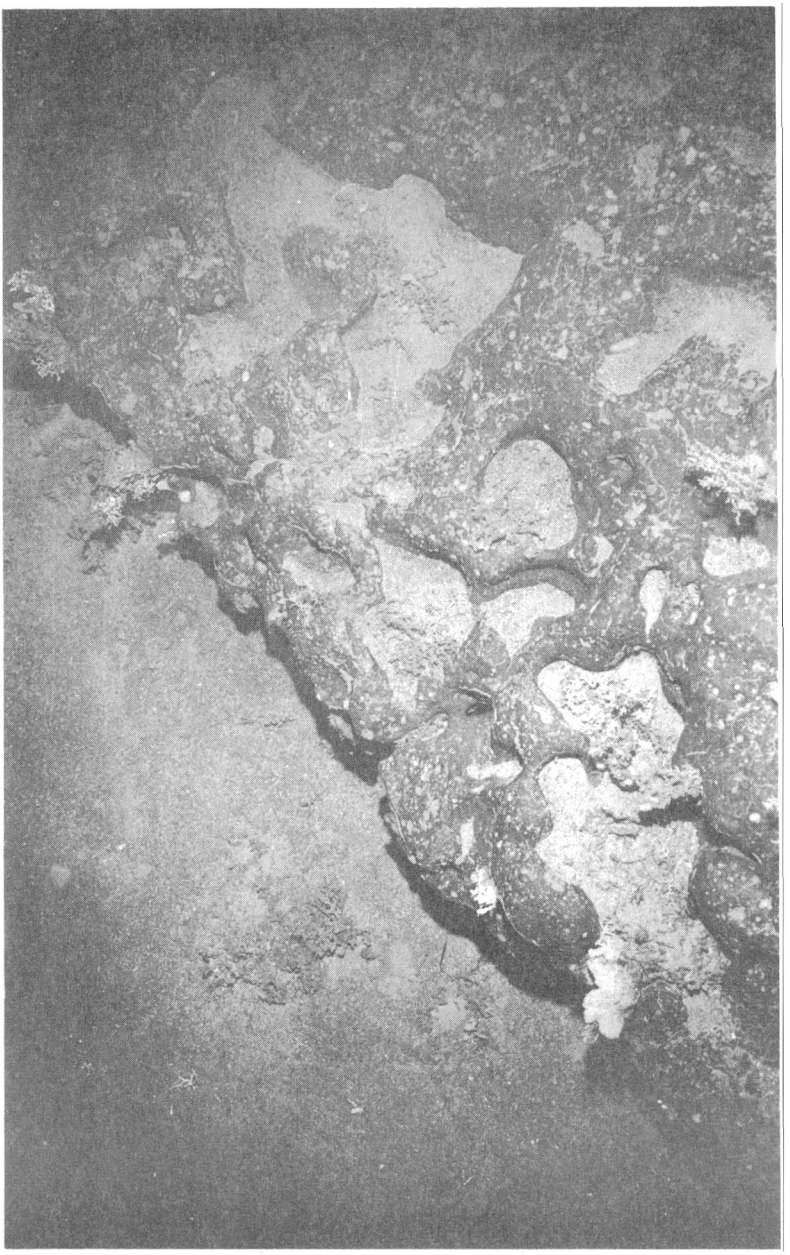

B

the pavement itself are siliceous worm casts. The ledge on photo B represents a vertical height of approximately 1 foot (calculated from camera-flash geometry and shadow width). Camera Station 'A', depth 480 fathoms, scale 15 x 11 feet.

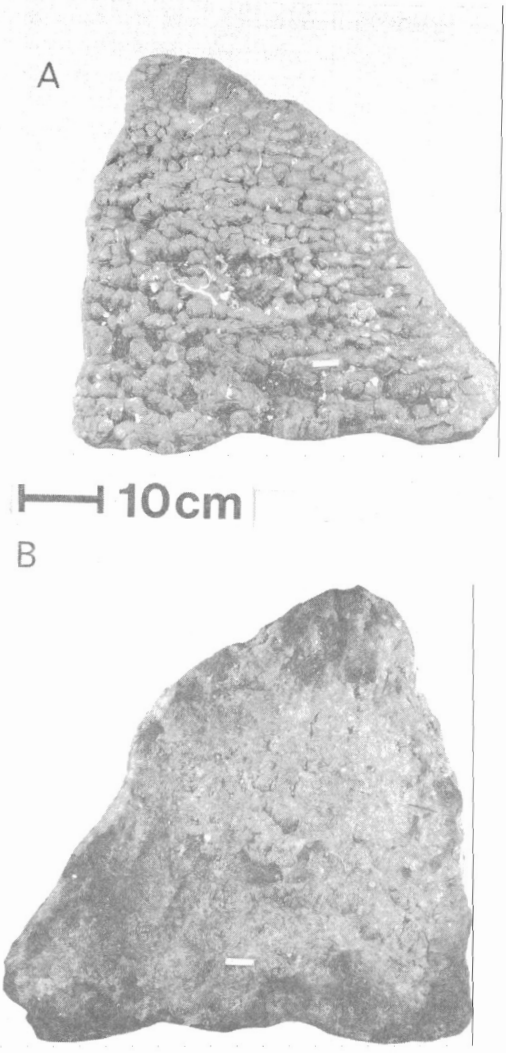

Figure 3A, B
Large (200-pound) specimen of ferro-manganese pavement recovered at station No. 54. A shows the convoluted top surface, with its fused nodular appearance; B shows the undersurface of the same specimen (AG-67-54-1).

down to 2, 400 fathoms showed that semiconsolidated ferro-manganese rich deposits covered the lower slopes of the seamount. A particularly large specimen was collected by the camera-dredge instrumentation (Aumento and Lawrence, 1968) at station No. 54 (Fig. 3). This bedded slab, weighing more than 200 pounds, is one of the largest ferro-manganese specimens ever collected. An erratic granitic boulder was also collected from dredge station No. 64. Altogether, three texturally different types of ferro-manganese deposits were collected; these are described below.

THE FERRO-MANGANESE DEPOSITS

1. Samples from the Crest Region

Samples from this region are characterized by the extremely compact ferro-manganese slabs from the top of the seamount (e. g. station No. 6). The slabs are very hard, glassy in appearance, with a conchoidal fracture, and perfectly bedded, and could easily be mistaken for the 'vitrain' of coal. The bedding is parallel and slightly wavy, and shows no sign of the concentric bedding generally attributed to manganese nodules. This indicates that they were deposited directly on the flat lava surfaces of San Pablo rather than around small nuclei. Every few millimetres there are thin continuous horizons (1 millimetre or less in width) of lithified carbonate material which contain abundant globigerina. The globigerina may be sufficiently distinctive to permit dating of the sediments and to make an estimate of the rate of deposition.

These ferro-manganese deposits are remarkably free from detrital sediment; the ferro-manganese content (Table 2) is comparable to that of samples from other stations, indicating that the top of the seamount is swept clear of sediments by the strong currents of the Gulf Stream. Samples from station No. 6 (see Table 1) gave only 2 per cent by weight of HCl insoluble residue, compared to up to 30 per cent for other samples. The impurities consist primarily of apatite, of possible authigenic origin.

2. Samples from the Middle Slopes

Samples from the middle slopes (e. g. station No. 54, Fig. 3) are porous and friable and thus resemble the common type of manganese nodule. Although well bedded, the bedding planes are often truncated by small 'neptunian' dykes infilled with Mn-poor material. Bedding planes consist of alternations of light and dark bands (Fig. 5). The thick slab 54-1 is unique in that it lacks a central nucleus; ferro-manganese slabs from other oceanic sources are generally composed of a zeolitic core and a thick, concentric ferro-manganese coating. Depositional nuclei are also completely absent in all other San Pablo deposits.

Table 1

Detrital mineral content of San Pablo ferro-manganese pavement

	Quartz	Plagioclase	Orthoclase	Apatite	Biotite	Amphibole	Hematite	Magnetite	Clinopyroxene	Chlorite	Kaolinite	Weight %
AG-65-1-1	++	++	+		-	-						20.3
AG-66-33-9	++	++	+		-	-	-					5.5
AG-67-C	++	++	-		-	-		+	+	-	-	32.9
AG-67-6-1				++			-					2.1
AG-67-54-1-1	++	++	+		-	-				-	-	3.8
AG-67-54-1-2	++	++	+		-	-				-	-	6.2
AG-67-54-1-3	++	++	+		-	-						11.1
AG-67-54-3-1	++	++	+		-	-				-	-	10.0

Note A: ++ = Major constituent
+ = Minor constituent
- = Trace constituent

Note B: Samples AG-65-1-1, a manganese nodule sensu stricto from the abyssal plains of the Atlantic Ocean, and AG-66-33-9, the manganese encrustation from basalts of the Mid-Atlantic Ridge, are also given for comparison.

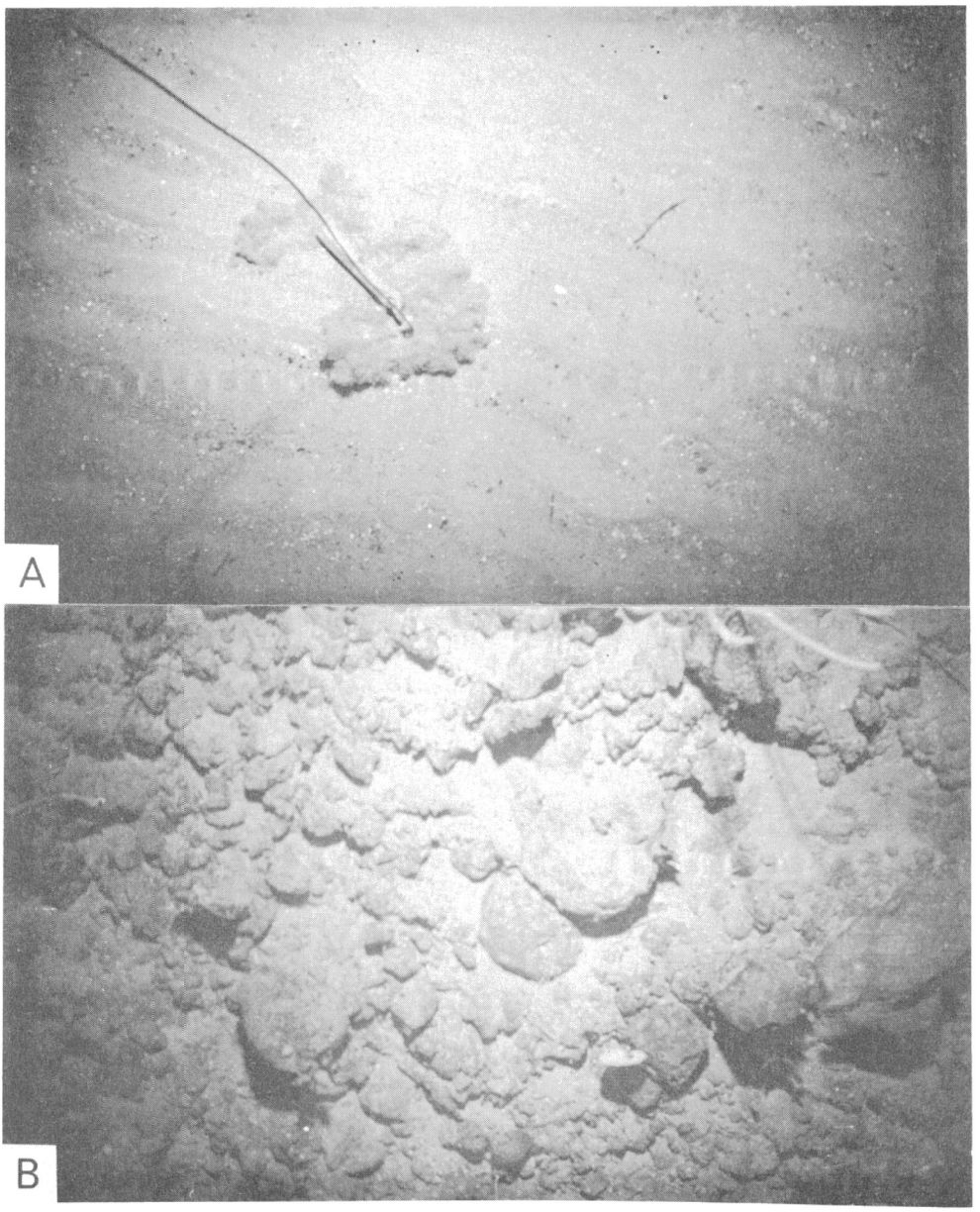

Figure 4A: Bottom photograph of current ripple-marks in sediments which fill small areas interstitial to the ferro-manganese pavement on the top of the seamount, camera station No. 43, depth 500 fathoms, scale 15 x 11 feet.

Figure 4B: Bottom photograph of screes on the lower slopes of San Pablo Seamount, Fragments are derived from basalt flows and ferro-manganese pavement higher up the slope. The fragments are covered by fine grained detrital material. camera station No. 53, depth 2, 850 fathoms, scale 15 x 11 feet.

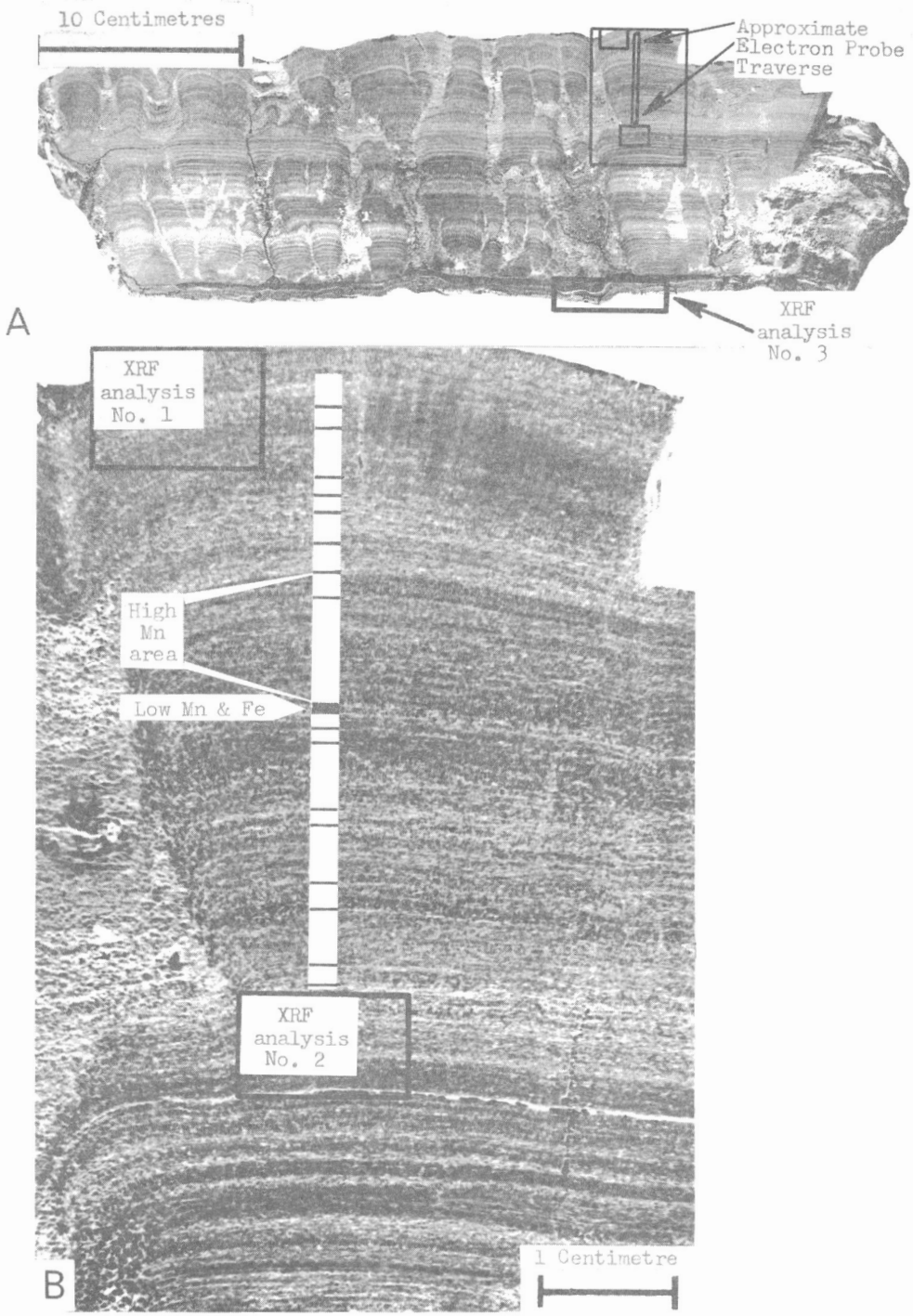
10 Centimetres
Approximate
Electron Probe
Traverse
XRF
analysis
No. 3
A
XRF
analysis
No. 1
High
Mn
area
Low Mn & Fe
XRF
analysis
No. 2
1 Centimetre
B

The reduced sweeping effect of the Gulf Stream at intermediate depths, together with an increase in detrital supply from the higher reaches of the seamount, results in a greater proportion of clastic sediments. These range from 4 to 10 per cent by weight, and are composed of quartz, plagioclase, and orthoclase, with numerous other minerals in trace amounts (Table 1). Apatite, the main detrital mineral in deposits from the crest region, is notably absent. The detrital minerals are similar to those contained within manganese encrustations of basalts from the Mid-Atlantic Ridge. An example of the latter type of encrustation is given in the tables for comparison (sample AG-66-33-9). The detrital material may therefore have a similar volcanic origin.

The pavement type deposits lack the well defined lithified carbonate layers of the shallower type (1) deposits; only one such layer exists near the base of the large slab (Fig. 5). The deposition of ferro-manganese and clastic material may be more continuous at these depths due to the reduced effect of minor variations in the Gulf Stream current on the various deposition rates. Calculations made from bottom photographs and dredged samples indicate that the continuous ferro-manganese encrustations of types (1) and (2) are at least one foot thick.

3. Samples from the Lower Slopes

Semiconsolidated sediments may extend from the lower slopes of San Pablo to the ocean deep at 2, 900 fathoms. As shown in Figure 4B, these sediments contain much detritus. Sample AG-67-C, obtained by piston coring, was found to contain 33 per cent detrital material and the largest assortment of minerals of any sample studied, though apatite is absent. The ferro-manganese content is correspondingly lower, but would be similar to that of the other types of deposits if calculated on a detritus free basis (Table 3). A manganese nodule sensu stricto from the abyssal plains of the Atlantic Ocean (sample AG-65-1-1) was the only one with a comparable amount of detrital material (Table 1).

Figure 5 A: Cross-section of specimen AG-67-54-1 (Fig. 3), showing good bedding within the pavement. Darker layers are generally enriched in Mn and Fe; the lighter bands are high in detrital or calcareous content. Rectangular areas represent locations from which material was removed for analysis.

Figure 5 B: Enlarge view of upper rectangle of Figure 5 A showing details of stratification and locations of bulk analysed samples and electron probe traverse. The latter is marked in white, with superimposed dark lines representing horizons of low Mn and Fe concentrations; the area bracketed represents an area with the highest Mn content.

Table 2

Bulk spectroscopic, X-ray fluorescence and colorimetric analyses of samples from the San Pablo ferro-manganese pavement

	AG-65 1-1	AG-66 33-9	AG-67 6-1	AG-67 54-1-1	AG-67 54-1-2	AG-67 54-1-3	AG-67 54-3-1	AG-67 C
B	.019	.020	.012	.017	.019	.017	.020	.019
Mg	.77	1.10	.70	.74	.84	.76	.75	.92
Al	2.0	1.4	.31	.83	1.2	.98	.76	2.1
Si	6.9	2.1	.88	1.1	2.3	3.2	1.4	8.0
K	.75	.41	.32	.47	.74	.74	.50	1.09
Ca	1.3	2.2	7.6	2.0	1.9	2.0	2.1	2.1
Sc	.0044	.0049	.0028	.0028	.0042	.0039	.0030	.0032
Ti	.60	1.1	.52	.55	.50	.55	.41	.65
V	.10	.13	.12	.15	.13	.16	.15	.085
Mn	13.7	14.0	16.1	16.4	16.1	13.5	16.7	10.9
Fe	19.4	19.8	13.0	19.3	18.6	18.5	19.1	15.8
Co	.15	.31	.20	.20	.22	.29	.22	.14
Ni	.12	.14	.13	.11	.25	.10	.13	.11
Cu	.090	.088	.065	.049	.058	.067	.061	.069
Zn	.060	.090	.090	.085	.090	.075	.080	.060
As	.021	.020	.019	.019	.025	.019	.019	.018
Sr	.091	.18	.24	.17	.16	.15	.18	.081
Y	.027	.060	.041	.025	.025	.029	.029	.019
Zr	.079	.11	.069	.079	.11	.089	.082	.056
Mo	.024	.039	.036	.037	.032	.028	.039	.020
Sb	.0025	.0035	.0045	.0060	.0045	.0025	.0035	.0010
Ba	.076	.13	.19	.16	.17	.12	.16	.086
Yb	.0033	.0054	.0038	.0033	.0032	.0039	.0036	.0027
Pb	.060	.061	.077	.057	.060	.064	.065	n.f.
L.O.I	20.9	28.8	24.0	33.9	30.8	31.6	28.9	16.9
HCl INSOL	20.3	5.5	2.1	3.8	6.2	11.1	10.0	32.9

Note: Samples AG-65-1-1 and AG-66-33-9 are given for comparison. Samples AG-67-54-1-1, 1-2, and 1-3 are from the top, centre and bottom of the large specimen AG-67-54-1.

Table 3

Chemical analyses from Table 2 recalculated on a detrital mineral free basis

	AG-65 1-1	AG-66 33-9	AG-67 6-1	AG-67 54-1-1	AG-67 54-1-2	AG-67 54-1-3	AG-67 54-1-3	AG-67 C
Mn	17.1	14.8	16.5	17.1	17.2	15.2	18.6	16.3
Fe	24.2	20.9	13.3	20.1	19.8	20.7	21.2	23.5
Co	.19	.33	.20	.21	.23	.33	.24	.21
Ni	.15	.15	.13	.11	.27	.11	.14	.16
Cu	.11	.094	.066	.051	.062	.076	.068	.10

CHEMISTRY

Previous Work

Theories on the formation and chemical characteristics of ferromanganese nodules have been put forward since the days of Dieulafait (1883) who believed that an organic mechanism, namely bacterial action, was responsible for the formation of these nodules. However, Graham (1959) showed that manganese nodules are especially low in organic content, thus excluding the possibility of bacterial action as a primary cause of deposition.

Buser and Grütter (1956) showed that the manganese in concretions was in the tetravalent form whereas most manganese in sea water is in solution as the divalent ion. This led Goldberg and Arrhenius (1958) to suggest that colloidal ferric iron at the sediment-water interface would oxidize and precipitate manganese to form various oxides. Once this has occurred, further precipitation of δ-MnO_2 would be induced by the catalytic action of previously deposited δ-MnO_2 as suggested by Ljunggren (1953) and Krauskopf (1957). Hence, on the assumption that seawater is the sole elemental source, the amount of Mn found in concretions may be related to the length of exposure of a surface layer of iron oxide, and hence to the rate of accumulation of iron. Similarly, due to the scavenging action of Mn for polyvalent ions with high charge densities, concentrations of Ni, Co, Cu, Pb and Mo would follow that of Mn. With rapid rates of iron accumulation, the exposure of the surface of a concretion to sea water would be short, resulting in little deposition of Mn and a low Mn/Fe ratio (0.10 or less). With slow rates of growth of the iron oxide layer, more Mn would be deposited and the Mn/Fe ratio would increase to 10 or more. This simplified hypothesis has not been substantiated

by the observations of Grant (1967) for the southern oceans. However, Rona et al. (1962) demonstrated in laboratory studies that the amount of Mn coprecipitated with Fe is inversely proportional to the rate of precipitation.

In contrast to the theory mentioned above, Arrhenius, Mero and Korkisch (1964) suggested that, assuming numerous elemental sources to be active, the specific origin of the elements might be determined by the Mn/Co ratio. A relatively slow concentration rate from sea water would result in a Mn/Co ratio of more than 300, while a rapid rate of deposition, due possibly to a volcanic source, might result in a Mn/Co ratio of less than 300. Arrhenius and Bonatti (1964), in contrast to Goldberg and Arrhenius (1958), suggested that Cu and Ni concentrations would be relatively higher in rapidly deposited volcanogenic concretions. This is due to the greater availability of crystallographic sites in the manganite minerals caused by structural disorder incurred in the rapid deposition and growth.

Mero (1962) was able to divide the Pacific Ocean Mn nodule occurrences into four main zones based on the Fe, Mn, Co, Ni, Cu and Pb concentrations, as follows:

(1) An Fe region where the ratio Mn/Fe is less than 1, and Fe/Co is high. This zone generally falls near the continental margins.

(2) An Mn region, where Mn/Fe is high, and concentrations of Ni, Co, Cu and Pb are low. This was taken to be a zone where a short time elapsed between the precipitation of Mn from solution in sea water and the agglomeration of manganese sols at the sea floor into nodules.

(3) A high Ni and Cu region farthest from land and nearest the Equator.

(4) A Co region on topographic highs in the Central Pacific.

There has been a recent impetus to the study of manganese nodules, possibly brought about by the proximity of the day when mining of these nodules will be commercially feasible. Presley, Brooks and Kaplan (1967) studied the interstitial waters of marine sediments to shed light on manganese nodule formation. They postulated the following sources for manganese: (a) leaching of detrital terrigenous sediments in continental shelf environments, (b) leaching of volcanic material in situ in volcanic areas, (c) injection from depth of metal-rich juvenile waters, and (d) biological concentration from seawater.

Biological activity is known to vary with the environment. It is highest in coastal sediments where reducing conditions enrich the sediments in Fe and Ni relative to the oxidizing areas of the deep seas. Co is slightly enriched in highly reducing areas only. In contrast, Mn is depleted in reducing areas, and concentrated in oxidizing areas.

Presley et al. (1967) found Mn to be enriched in the interstitial waters of deep-sea cores. The Mn is thought to diffuse from depth to the surface, either along concentration gradients or by compaction of sediments. On reaching the water-sediment interface, the Mn would be oxidized to MnO_2 by the presence of dissolved molecular oxygen rather than by the catalytic action of Fe, as suggested by Goldberg and Arrhenius (1958). Colloidal MnO_2 would then accrete with iron oxides and subsequently catalyze the precipitation of Ni and Co.

Price (1967) compared deep-sea pelagic nodules with those of shallow water lacustrine or neritic environments. He found that whereas the Mn/Fe ratio is generally dependent on factors other than depth, ease of precipitation and retention of Fe relative to Mn in near-shore areas may produce an increasing Mn/Fe ratio with depth for localized areas (supporting in part, the existence of Mero's Zone '1' of the Continental Margins). Metal relations were thought to be dependent on conditions of deposition: e.g. in the Black Sea Mn is followed by Ni, Co, Cu, and Mo, and Fe is followed by P, whereas in oceanic regions Fe is followed by Co, and Mn by Ni and Cu only.

Price (op. cit) also remarked on the importance of organic matter. The seaward depletion of organic matter in sea water causes a corresponding thickening of the oxidized upper sediment layer. This transgression is of importance, because Lynn and Bonatti (1965) showed that where a reducing layer underlies oxidizing sediments (i.e. in marginal areas of the Pacific) there is a considerable upward mobility of Mn from the reduced sediments to be largely concentrated in near-surface oxidizing layers. This mechanism would produce higher Mn/Fe ratios in deposits of continental margins in contrast to the observations of Mero (1962); in open seas, with sediments of low organic content and a mineral reduced layer, there would be a slower migration of elements through the oxide layer, resulting in slower overall deposition rates and lower Mn/Fe ratios.

Jenkyns (1967) observed persistently greater Fe contents over those of Mn in fossil ferro-manganese nodules from Sicily. He attributed this to a post-depositional migration of the more mobile Mn. He also found high Ca values, possibly due to the formation of these nodules in a former limestone environment. Deposition was thought to have occurred in a shallow water environment on top of transient topographic highs, similar to the non-magnetic seamounts now occurring off the Iberian coast.

Chemistry of the San Pablo Deposits

Representative samples of the three types of deposits found on San Pablo Seamount were analyzed for 24 major and minor elements. Results (Table 2) include, for comparison, analyses of a manganese nodule (AG-65-1-1) and of manganese encrustation on basalt pillows from the Mid-Atlantic Ridge (AG-66-33-9). Table 3 gives the more important metal concentrations

recalculated on a detrital mineral free basis. The elements Si, K, Ca, Ti, Mn, Fe, Co, Ni and Cu were determined by X-ray fluorescence techniques (dilution with fusion, spiking and direct comparison; analyst, F. Aumento); the elements Zn, As and Sb were determined by J. J. Lynch of the Geochemistry Section, Geological Survey using colorimetric techniques; and the remainder were determined by the Emission Spectroscopy Group of the Analytical Chemistry Section, Geological Survey. Results from the latter also provided confirmations on some of the element concentrations determined by Aumento and Lynch.

The elements Al, Si, K and Ca show the main concentrational variations between analyzed bulk samples (Table 2); however, these variations are directly related to the concentrations of detrital material. For example, sample AG-67-6-1 with a high apatite content, has an abnormally high Ca concentration. Similarly, increasing amounts of insoluble material from the top of specimen AG-67-54-1(-1) to the bottom (-3) can be correlated with increasing concentrations of Si, Al and K. Table 3 shows that when the analyses are recalculated on a detrital mineral free basis, then the Fe, and especially the Mn concentrations become remarkably constant. The only significantly different sample is AG-67-6-1, which has an Mn/Fe ratio greater than 1. The remaining elements (Table 2) have constant concentrations also, with only the Mid-Atlantic Ridge sample showing a general enrichment in Ti, Co, Y, Zr and Yb, possibly due to its close association with recent volcanic activity. Therefore, it seems that the rate of deposition of most of the constituents of these deposits does not vary appreciably over the San Pablo Seamount. The Fe concentration, however, appears to increase with depth: Fe is lowest (13 per cent) in sample AG-67-6-1 from the top of the seamount, intermediate in AG-67-54-1 and highest (24 per cent) in the core sample AG-67-C from 2,400 fathoms.

If the Fe concentration had been dependent on the reducing state of the underlying sediments (Presley, et al., 1967), one might have expected the reverse trend to appear: i.e. with increasing depth and decreasing reduction in the sediments, the Fe concentration might have shown depletion also. However, it is not known whether there are sediments beneath the San Pablo manganese pavement; it is more probable that the underlying rocks are lava flows which would not be subject to organic influences. Under these conditions the hypothesis of Presley et al. on biogenical control may not be strictly applicable.

The iron concentration variations do, on the other hand, fit the explanations offered by Price (1967) on the variations in oxide layer thickness and the resultant Mn/Fe ratios. The hypotheses of Presley et al. and Price are based on the same basic fact: the reduced sediment layer decreases in thickness with depth; they draw, however, opposing conclusions, one of which fits the observations on San Pablo (Price), the other the observations of Mero (Presley, et al.).

The compositions, compared to the average composition of nodules from the Pacific and Atlantic Oceans (based on 54 samples from the Pacific and 4 from the Atlantic; Mero, 1962), are generally low in Al, Mg, Si, and Ti (due to their low detrital mineral concentrations), also low in Ni, B, Cu, Zr and Pb, average in Ca, K, Mn, Co, Ba and Yb, and high in Fe, Se, V, Sr and Y.

It would appear that the deposition rate on San Pablo Seamount, inferred on the basis of the Mn/Fe ratio, is relatively slow throughout, but increases slightly with depth. Indeed, a direct relationship can be made between the depositional rate and depth. However, the data suggest that the rate of Mn deposition is constant throughout the seamount, while the Fe deposition rate varies. Similarly, the metals thought to be associated with Mn, namely Co, Ni and Cu, show little or no variation in concentration over the seamount. The original relationships suggested by Goldberg and Arrhenius (1958) would therefore also seem to hold true here. In contrast, the Mn/Co ratio, which varies from a low of 46 to a high of 84, would indicate (after Arrhenius and Bonatti, 1964) a rapid concretion rate typical of volcanogenic depositions. This is in keeping with the volcanic nature of the seamount, but is in direct contrast to the relatively slow rate of concretion suggested by the Mn/Fe ratio.

If the San Pablo deposits are classified according to the zonal subdivision used by Mero (1962) in the Pacific Ocean, they fall, with the exception of the crest deposits, into zone (1). This zone represents deposits from continental margins, and is hardly in keeping with the setting of San Pablo. The crest deposits (e.g. AG-67-6-1) are transitional between types (1) and (2) due to their higher Mn/Fe ratio but moderate Ni, Co, Cu and Pb concentrations. The sample from the Mid-Atlantic Ridge falls into zone (1). This suggests that either a single sample is insufficient for the classification of a manganese deposit, or that the Mid-Atlantic Ridge may have had the same effect as a continental mass on the ferro-manganese depositional ratio.

These problems are caused by the scarcity of samples upon which the hypotheses are based. Each hypothesis may only be correct in very localized conditions, and conclusions on chemical and depositional criteria should not be applied to whole oceans on the basis of results from a few scattered samples. Even the closely spaced samples from the restricted area of San Pablo Seamount may provide insufficient information. Knowledge as to what directly underlies the manganese pavement on San Pablo Seamount is lacking. The pavement may not lie directly on top of the lava flows which are thought to constitute the main core of the seamount, since some of the bottom photographs show indications of a sedimentary layer beneath the pavement. This sedimentary layer may be continuous or only local in nature; it may be the topmost in an alternation of layers of manganese pavements and sediments or it may be unique. These questions will have to be answered before final conclusions can be made on the depositional mechanisms over the seamount.

MINERALOGY

The ferro-manganese deposits consist of a number of intimately and randomly intergrown phases of various compositions. Not all phases are crystalline; indeed, the majority are amorphous gels. Table 4 lists some of the phases detected in natural and synthetic ferro-manganese material by Buser and Graf (1955), Buser and Grütter (1956), McMurdie (1944), Burns and Fuerstenau (1966) and others. Burns and Fuerstenau (op. cit.) have noted the confusion which arises between chemical and mineralogical usage of names given to phases.

The generally poor crystallinity of these phases, together with the similarities of their physical characteristics (as seen in Table 4), makes identification difficult. A combination of X-ray, chemical and electron microscope observations is commonly necessary to identify the intimate admixtures found in the ferro-manganese deposits, but even so it does not always result in conclusive identifications.

X-ray Observations

The San Pablo samples were repeatedly scanned on an X-ray diffractometer in attempts to obtain diffraction patterns. In addition, exposures of 20 hours on a focusing Guinier camera and of 80 hours or more on a 57.34 mm diameter Debye-Scherrer camera were attempted.

The few peaks obtained were accounted for as belonging to the detrital minerals. Extra peaks consisting of a broad band between 4.21 Å and 4.13 Å, a line at 2.45 Å, and a second broad band between 1.43 Å and 1.41 Å occurred in all the samples investigated. The 2.45 Å and 1.43-1.41 Å peaks are the (100) and (110) reflections of δ-MnO_2, and not those of the ferrous manganites, since the higher d-spacing lines at 9.7 Å and 4.8 Å for the latter are absent. The band at 4.21-4.13 Å is due to the vaseline binder used in mounting the specimens, plus an extremely weak and diffuse superimposed main line of poorly crystalline goethite (α-FeOOH) at 4.21 Å.

The bulk of the ferro-manganese deposits from San Pablo Seamount are therefore amorphous to X-rays, with only very small amounts of the crystalline δ-MnO_2 phase appearing in diffractograms. In order to detect other crystalline phases, in concentrations too low for observation by X-ray diffraction, samples were further examined by electron microscopy.

Electron Microscope Observations

Samples were ground to less than one micron size in ethyl alcohol, and then vibrated ultrasonically in suspension to ensure good particle dispersion. One drop of the suspension was then pipetted onto a microscope sample

grid (previously coated with a 300 Å -thick carbon layer) and allowed to dry. The resulting sample mounts were used for electron microscopy and for selected area electron diffraction.

Electron microscopy revealed a number of different morphologies of the dispersed particles. Although most samples contained at least some of each morphological type, preliminary observations showed that certain phases were more characteristic of some particular types of deposits. The dispersed state mineralogy is as follows:

(1) By far the most common particle morphology is an agglomeration of grains (Fig. 6A); the individual particles are featureless and ill-defined, without morphological characteristics. When these grains are especially thin, high magnifications (x 70, 000) show them to be of an open, rather porous structure. These particles do not give single crystal diffraction patterns; any polycrystalline patterns present must be so weak as to be indistinguishable from the polycrystalline pattern of the carbon substrate; the latter is by necessity always present, and its diffraction pattern is always superimposed onto other patterns under examination.

(2) Grading into particles of type (1) are other grains which appear to have dispersed further; these show the morphology of the components which build up the larger grains described above. Mesh structures of very thin fibres, not more than 80 Å thick (Fig. 6B) are visible; the fibres are of variable length, straight or curved, and far too small to give individual diffraction patterns. The bulk of the mesh does not give a diffraction pattern either.

(3) Dispersed at random throughout particles (1) and (2) are a number of thin flakes. These are extremely thin overlapping laminae of anhedral shape. The flakes give diffraction patterns, generally a number of superimposed single crystal patterns, as a result of the stacking of many plates. The electron diffraction patterns show a hexagonal or pseudo-hexagonal symmetry and allow at least three different phases to be identified:

(a) Flakes (Fig. 7A) giving a diffraction pattern with a true hexagonal symmetry and a = 2.4 – 2.5 Å (Fig. 7B) are identified as the δ-MnO_2 phase, which, although predominant in all the San Pablo deposits, is more common in specimens from the higher reaches of the seamount (e. g. sample AG-67-6-1).

(b) Thin superimposed flakes give an almost polycrystalline pattern, from which can be discerned hexagonal symmetry with a = 2.1 Å. The value obtained for 'a' is too low for δ-MnO_2, and cannot be matched to other known manganese or iron minerals. These flakes occur predominantly in sample AG-67-6-1.

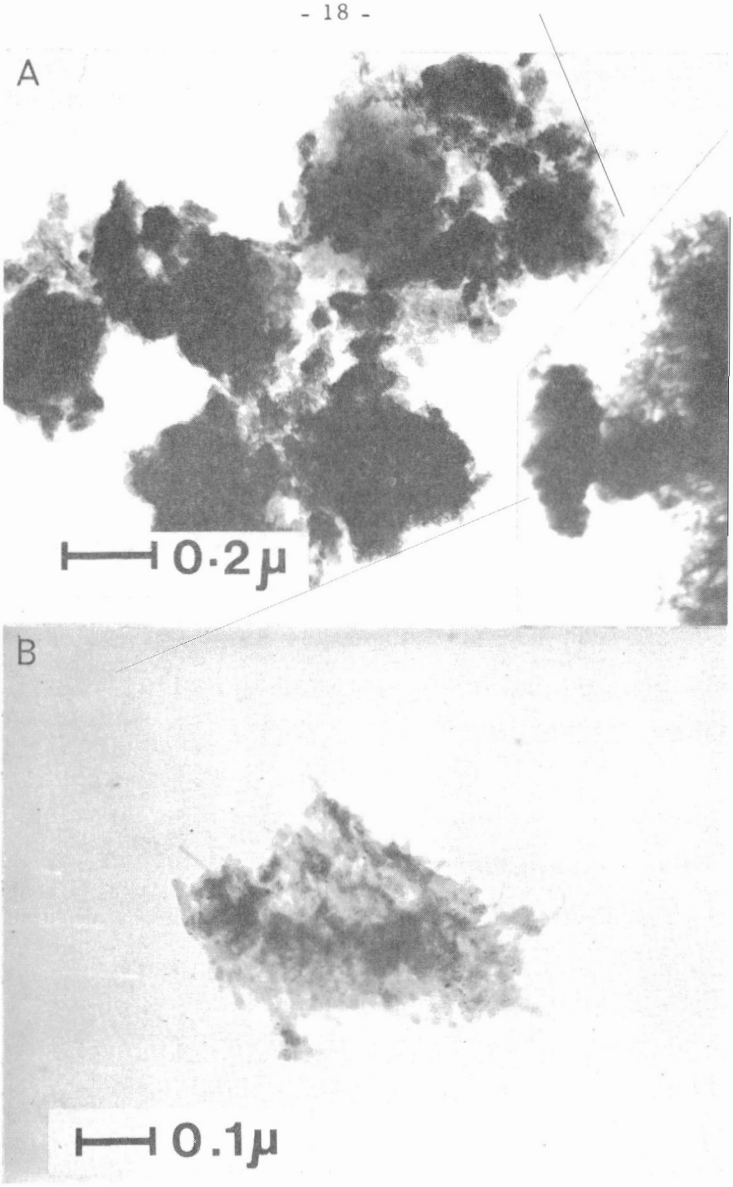

Figure 6A: Electron micrograph of featureless, amorphous ferro-manganese phases. They appear to have a porous consistency.

Figure 6B: Mesh structure of very thin fibres which in many cases make up the featureless grains shown in A. The fibres are less than 80 Å thick, and are too small to give electron diffraction patterns (if crystalline).

(c) Common throughout the deposits, especially in the deeper ones, are thin flakes (Fig. 8A) giving pseudohexagonal electron diffraction patterns (Fig. 8B). However, the distribution of intensities of reflections indicates that a lower symmetry is present, with cell parameters 8.8 Å and 5.2 Å. These are the 'a' (= 8.8 Å) and 'b' (= 5.2 Å) parameters of the monoclinic (β = 90°) mineral $Mn_2O_3.H_2O$.

(4) Particles with a lath-like or even tubular morphology (Fig. 9A) occur in intimate association with the flakes and grains described above. The laths give the characteristic 'rotation' electron diffraction patterns of crystals with tubular morphology. The cell dimensions are 5.3 Å, 8.9 Å and 14.3 Å; these are very close to the parameters of the serpentine mineral 'chrysotile' with a = 5.32 Å, b = 9.2 Å and c = 14.6 Å. The fibrous manganous manganite (Table 4) $MnO_2.Mn(OH)_2.2H_2O$ is a two layered hexagonal mineral with unit cell dimensions a = 5.82 Å and c = 14.62 Å. Should there occur a mismatching of the two layers, then the layers could curl as a strain relief mechanism (as occurs in chrysotiles). This would result in a pattern very similar to that obtained. However, such a mechanism has not been reported in manganites before, and for lack of further evidence at present, it is assumed that the fibres are indeed those of the serpentine mineral chrysotile. The electron diffraction patterns are therefore interpreted as due to intimate admixtures of ortho- and clino-chrysotiles in varying proportions (Fig. 9B). The presence of chrysotile in these deposits is unusual, and was at first attributed to contamination of the specimens. However, once that possibility was eliminated by repeated sample preparation under controlled conditions, it was concluded that the chrysotile is either authigenic, forming contemporaneously with the ferro-manganese deposits, or is a detrital mineral originating from the serpentinized basalts which may make up the slopes of San Pablo Seamount.

Electron microscope observations are in good agreement with the X-ray data. Both suggest that the bulk of the material is amorphous, with only trace amounts of crystalline δ-MnO_2 and even smaller amounts of $Mn_2O_3.H_2O$ present. The concentration of chrysotile is so low that it is impossible to detect by X-ray diffraction. Conversely, any goethite present is so poorly crystalline that it cannot be detected by electron diffraction. Neither the 10 Å nor the 7 Å ferrous manganites were detected by either techniques; if these are present, they may also be in an almost amorphous state.

These preliminary observations suggest that the manganese oxide type may vary with depth of the deposits on the seamount. A higher oxidation state may have produced the δ-MnO_2 phase, predominant on the higher reaches of the seamount, with its associated low Fe deposition rates whereas more reducing conditions in the lower reaches may have favoured the formation of $Mn_2O_3.H_2O$ and higher Fe deposition rates.

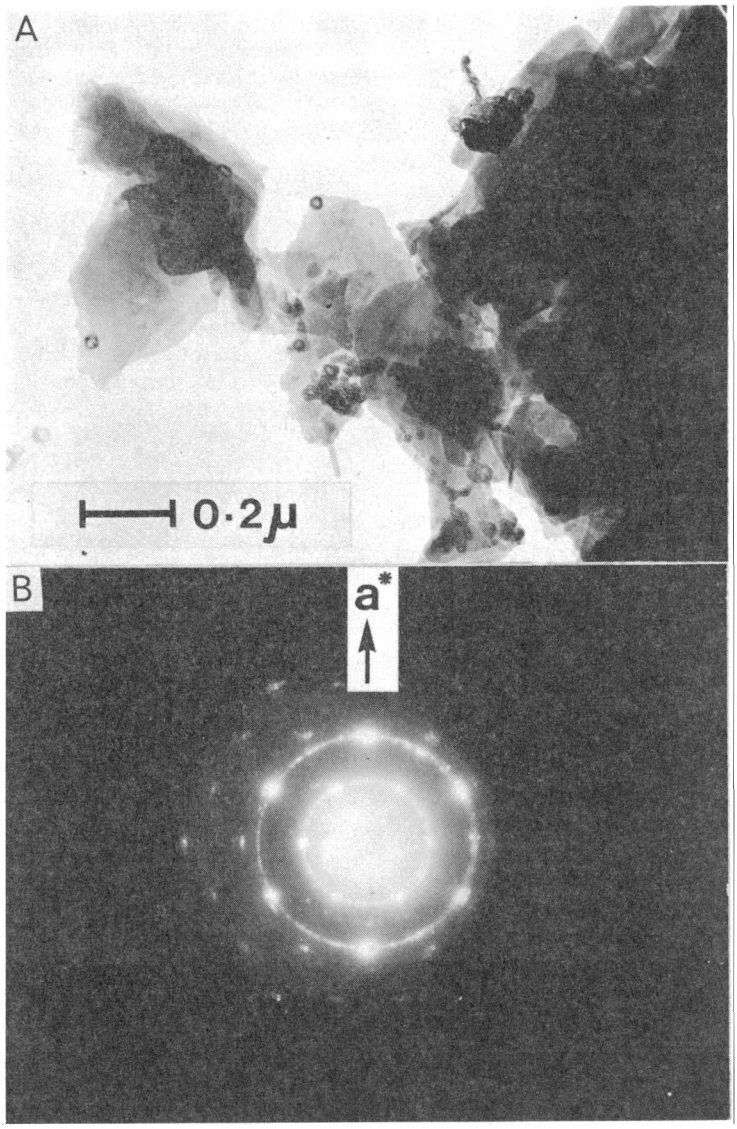

Figure 7 A: Electron micrograph of extremely thin, overlapping anhedral plates. They give electron diffraction patterns, as reproduced below.

Figure 7 B: Electron diffraction pattern of plates with a hexagonal symmetry. a = 2.4 - 2.5 Å; has been identified as δ-MnO_2.

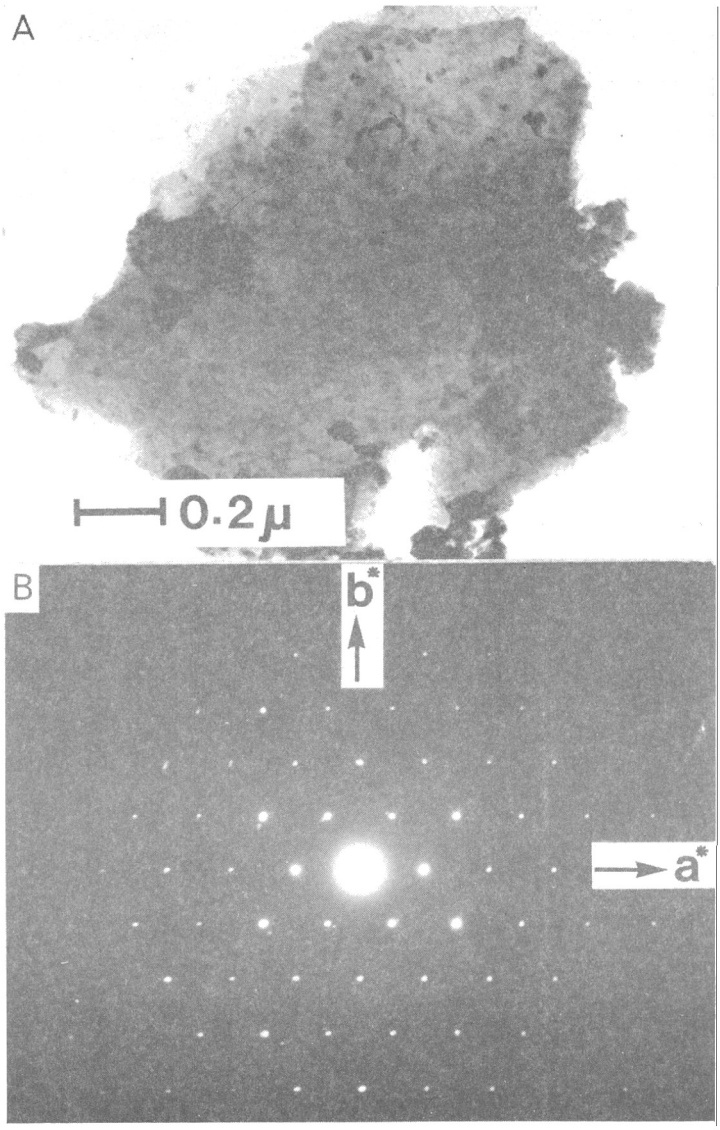

Figure 8A: Electron micrographs of thin flakes of $Mn_2O_3.H_2O$. These give good electron diffraction patterns.

Figure 8B: Electron diffraction pattern of flakes shown in 8A, with pseudo-hexagonal symmetry (a = 8.8Å and b = 5.2Å). This is the monoclinic ($\beta = 90°$) manganous manganite $Mn_2O_3.H_2O$.

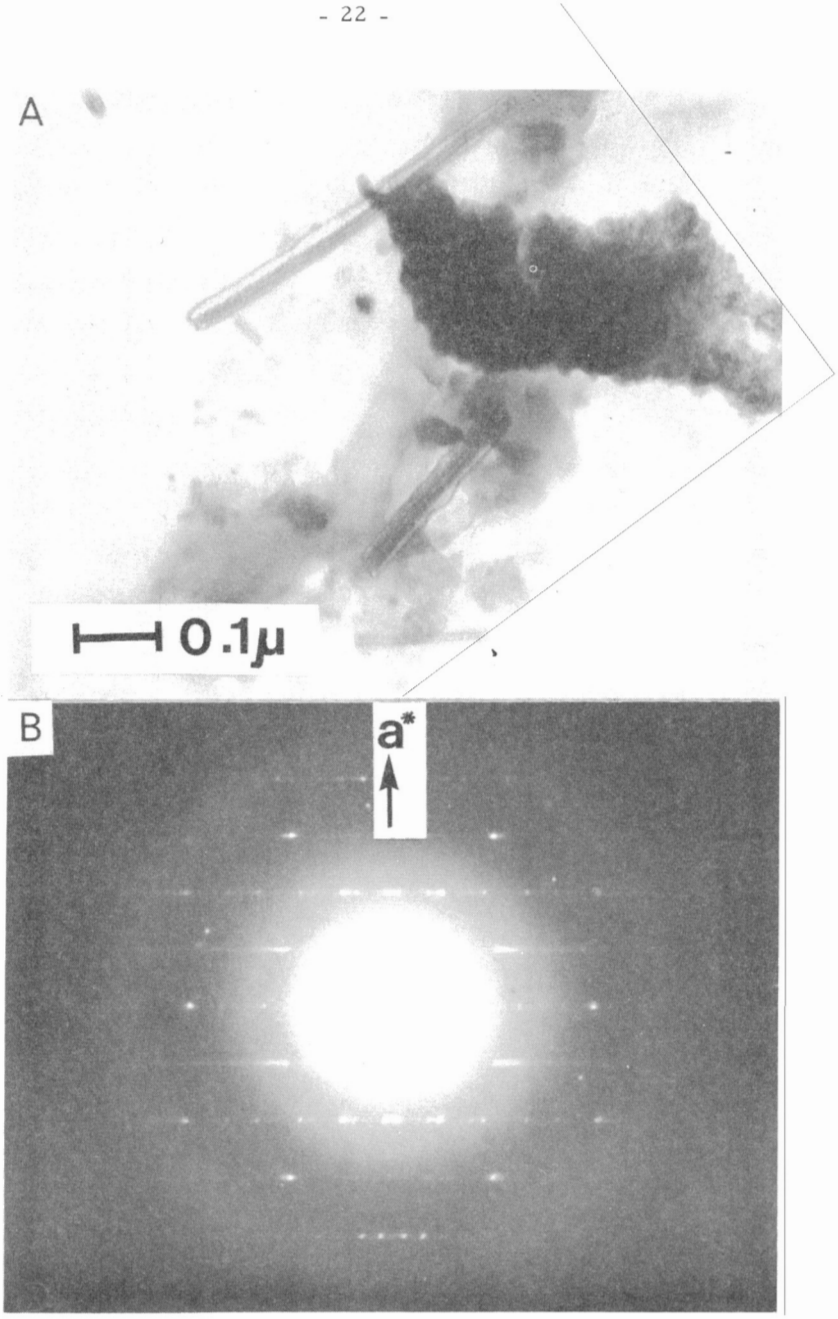

Figure 9A: Electron micrograph of lath-like or tubular chrysotile fibres coexisting with the ferro-manganese minerals.

Figure 9B: Electron diffraction pattern of chrysotile fibres in 9A, showing characteristic 'rotation' diffraction pattern with a = 5.3Å, b = 8.9Å and c = 14.3Å. The pattern shows a superimposition of both ortho- and clino-chrysotile fibres.

ELECTRON PROBE MICROANALYSIS

The hypotheses discussed in the preceding section on 'Chemistry' are based solely on bulk chemical analyses of the ferro-manganese deposits. These analyses do not take into consideration the admixtures of different mineral phases, the detrital mineral contamination, the chemical variations between light and dark bands and other microscopic variations.

Burns (1965) and Burns and Fuerstenau (op. cit.) have undertaken closer investigations into the problems of inter-element correlations. They employed electron-probe techniques (electron beam scanning and specimen traversing) to study inter-element relationships, and to correlate these to the different mineralogical phases. Measurements over 350μ square areas on manganese nodules from 14 different localities gave consistent results, which can be summarized as follows:

(1) The Fe concentration is variable, whereas the Mn is relatively uniform throughout a nodule. Mn is slightly higher where Fe is low.

(2) Co, Ti and Ca are high in high Fe regions. These occur where δ-MnO_2 and $FeOOH.nH_2O$ are the predominant phases. Cobalt may substitute for ferric iron in the hydrated iron oxide phase $(Fe, Co)OOH.nH_2O$.

(3) Where Mn is high, Al is also high, as are Ni, Cu, Zn, Mg, K and Ba. These are thought to be contained in the 7 Å manganite phase.

Electron Probe Techniques

The large slab AG-67-54-1 was selected for electron probe analysis because it offered an uninterrupted, perfectly bedded cross-section over a thickness of 12 centimetres. A vertical section at right angles to the bedding approximately 1 centimetre thick and 5 centimetres long was cut from the top of the specimen (see Fig. 5); the column was cleaved along bedding planes into five pieces, and each piece embedded in a 1-inch diameter specimen holder. The surfaces to be examined were ground using a lap impregnated with 6 micron diamond powder, and were then impregnated under vacuum with hot, fluid epoxy. Further grinding and polishing with 1 micron diamond paste was then resumed. Impregnation permitted a satisfactory degree of polishing to be attained; this had proved impossible previously on untreated samples due to their friability and softness.

A thin film of evaporated carbon was used to make the specimen surfaces conducting. Quantitative measurements for Fe, Mn, Ni and Co were made on an MAC electron probe fitted with two spectrometres.

Different analytical methods were evaluated at first to ascertain which were best suited to the problem at hand. Eventually the following techniques were employed.

(1) Spot counting for the elements Mn and Fe every 50 to 200μ along a 4.6 centimetre traverse from the top of the specimen down the deposition sequence. An electron beam diameter of 10μ was employed for the spot counts. Standards (Fe and Mn metals, hematite and rhodonite) were read at regular intervals between every few readings on the ferro-manganese specimens. Intensities measured on the specimens were corrected by comparing the intensities obtained from the standards at that particular time to the intensities obtained on the standards at the beginning of the investigation. Although the intensities from the standards never varied by more than 12 per cent of the maximum counts over a number of days, use of the correction ensured a constant reference point which permitted direct comparison of concentrations to be made. A total of 461 points, with an average separation of 100μ, were analyzed along the 4.6 centimetre traverse for both Mn and Fe. Background readings for Mn and Fe were also taken every 10 or so peak readings; these did not show any significant variation throughout the specimens. These results, converted to percentage compositions, are plotted in Figure 10 (at back of report).

(2) An area as free as possible from cracks, holes, blemishes, inclusions, etc., from near the centre of the traverse was selected (see Figs. 5 and 10) for a line scan. The specimen was traversed for a distance of about 900 microns at a speed of 10 microns per minute under an electron beam of about one micron diameter. The electron beam left a clearly visible mark on the specimen surface, and tests showed that several traverses could be made along the same line without noticeable damage to the surface or any effect on the quantitative results. One spectrometer was set on the Fe $K\alpha$ peak and the second one was set for successive traverses on Mn $K\alpha$, Co $K\alpha$, Ni $K\alpha$ and background settings. The Fe $K\alpha$ peak thus served as a reference to which the other data might be compared. Results for the elements Fe, Mn, Co and Ni are plotted on Figure 10. It should be noted that whereas the percentage concentration traces for Fe and Mn are direct reproductions of the spectrometer outputs on the strip-chart recorders, those for Co and Ni are the net result of subtracting the background traces for these elements from their peak traces. The small concentrations of Co and Ni present necessitated this correction: the background beneath their respective $K\alpha$ peaks was far too dependent on the variations in Fe concentration to be left uncorrected. The subtraction was computed manually by measuring the trace heights above zero every 2-3μ for both peak and background spectrometer outputs and subtracting one value from the other. Because of the inherent errors of such a method, no importance should be attached to the minor fluctuations seen on the resultant graphs plotted on Figure 9; only major peaks and traces are of significance.

Electron Probe Results

In addition to the spot counting and line scan graphs, Figure 10 shows two additional plots for Mn and Fe. These show the concentration values in percentages averaged every 100μ from the spot counts, in an attempt to show the general variation trends for Mn and Fe rather than the finer details.

The average value plots show that the Fe concentration, with its minor fluctuations, remains relatively constant between 20 and 25 per cent, whereas the Mn concentration shows more definite zones of enrichment (16-21 per cent) and depletion (13-17 per cent). There also appears to be little correlation between the Mn and Fe values: in places an increase in Fe concentration is accompanied by a decrease in Mn (e.g. 0-2 millimetres from the top, 1.9-2.1 centimetres from the top, and elsewhere), elsewhere there is an equally marked sympathetic variation between the two elements. However, whereas the specimens do not show any optically detectable variations where the Mn concentration is antithetical to that of Fe, parallel Mn and Fe concentrations (which always commence with both concentrations in a decreasing trend) can be attributed to definite flaws on the specimen surfaces (generally epoxy filled cracks, detrital minerals, etc.). The antithetical variations between Mn and Fe may therefore be more significant than the sympathetic variations.

Both the indications of more constant Fe values, compared to Mn, and the antithetical Mn and Fe concentration variations are in contrast with the results of Burns and Fuerstenau (1966), who found more constant Mn values, with only a very slight increase in Mn in areas of markedly reduced Fe concentration.

The spot count plots are even more revealing. They show a remarkable and unambiguous correlation throughout the traverse between high Mn values and low Fe values, and vice versa. Those spots which show both low Fe and Mn values can be readily correlated with locations on the specimen surfaces where there occur surface imperfections, inclusions, or bands of very light colour. Some of these bands, which show up clearly in hand specimen and on probe analysis, are shown on Figure 5. Also marked is a particularly dark zone, about 1 centimetre wide, which gives the highest Mn values (from approximately 1.5 to 2.5 centimetres from the top).

Increases and decreases in Mn concentration levels are gradual, and appear to be cyclic. The top of the specimen, representing the present conditions of deposition, indicates a period of high Mn deposition. If eventually we succeed in dating these deposits with accuracy, we may be able to correlate these Mn fluctuations with known events in the past (e.g. Grant's, 1967, correlation with ice ages).

Although the 10μ diameter electron beam may be analyzing more than one mineral phase at any instant, there appear a number of recurring Mn/Fe

concentration combinations. These may be due to the presence of different mineral phases, or different admixtures of mineral phases under the electron beam. Listed in decreasing order of Fe concentration, these appear to be as follows:

(1)	Fe	32-33 per cent	Mn	5-7 per cent
(2)		27-29 per cent		11-13 per cent
(3)		18-21 per cent		16-20 per cent

Only the latter combination may have an equivalent in the nodules analyzed by Burns and Fuerstenau (1966), who interpreted zones with approximately 23 per cent Mn and 10-20 per cent Fe as containing mixtures of δ-MnO_2 and FeOOH. If this deduction can be applied to the San Pablo Pavement, there would appear to be an enrichment of an amorphous FeOOH phase throughout the sequence, with especially high degrees of enrichment along certain lighter coloured horizons. Unfortunately, it is not possible to determine the phases present (see 'Mineralogy', p. 13 and following), except to the extent of being able to exclude the existence of crystalline 7 Å or 10 Å manganite phases. Any correlation of composition with mineral phases is therefore purely speculative.

The line scan of that part of the traverse approximately 15 millimetres from the top of the slab (Fig. 10, top) provides further confirmation of the antithetical variation between Mn and Fe. The two spots where there are marked drops of both Mn and Fe concentration are both due to visible cracks on the surface of the specimen. The different levels in concentration may be due to the following possibilities: (a) the existence of different phases of different compositions, (b) a continuous variation in the proportions of two intimately admixed phases of constant composition, one rich in Fe, the other in Mn, (c) a single phase with continuous chemical variation between Mn and Fe end members. Amorphous ferrous manganites may be capable of having continuously variable compositions between the known end members with Mn: Fe ratios of 2:1 and 3:1. This could explain the variations detected, but would require the additional intimate admixture of constant amounts of a pure Fe phase (e.g., amorphous $FeOOH.nH_2O$) to raise the calculated Fe concentration to the levels measured.

Both Co and Ni show sympathetic variation with Mn, and are hence antithetical to Fe. Such trends are not as marked as the antithetical variations between Mn and Fe; this is due to the low concentrations and corrections involved (see above). However, both the major highs and major lows of Mn can be correlated to the respective highs and lows of Co and Ni. The antithetical variation of Co with Fe disagrees with the correlation reported by Burns and Fuerstenau (1966), whereas that of Ni is in agreement with their findings. Co and Ni must therefore be associated with a Mn-rich phase, more in agreement with the hypotheses of Goldberg and Arrhenius (1958) and Presley et al. (1967), rather than with the hypothesis of Arrhenius et al. (1964) and the observations of Price (1967) and Burns and Fuerstenau (1966).

SUMMARY AND CONCLUSIONS

The crest and flanks of San Pablo Seamount are completely enveloped by an extensive ferro-manganese pavement. The pavement is well bedded throughout and lacks the depositional nuclei characteristic of manganese nodules. Three types of deposits have been found: the hard, glassy slabs from the crest regions, the massive, more friable deposits from the flanks, and the semiconsolidated sediments rich in detrital minerals from the lower slopes.

Chemical analyses of bulk samples, recalculated on a detrital mineral free basis, show remarkably constant Mn concentrations throughout the deposits, whereas Fe concentrations can be shown to increase with depth. Compared to other known manganese nodules, Fe concentrations are generally high, whereas the minor elements usually associated with ferro-manganese deposits occur in relatively low concentrations. A number of ambiguous deductions as to the depositional history of the San Pablo pavements are reached when trying to evaluate the ratios of various metal concentrations in the light of existing depositional hypotheses; it is suggested that existing hypotheses are all too commonly based on insufficient sampling data.

X-ray and electron microscope observations have revealed a number of phases. Only two of the manganese minerals, namely δ-MnO_2 and $Mn_2O_3.H_2O$ are crystalline; the remainder, together with the iron phases, are amorphous to X-rays and electron beams. The phases most common in ferro-manganese deposits, the 10 Å and 7 Å manganites, are completely absent here. The type of manganese oxide appears to vary with depth of deposition: a higher oxidation state on the higher reaches of San Pablo may favour the formation of δ-MnO_2, whereas a lower oxidation state in the lower reaches of the seamount may favour $Mn_2O_3.H_2O$ together with higher concentrations of amorphous iron phases.

Electron probe analyses over a short distance (4.6 centimetres) across the bedding of the pavement have revealed the following: (a) the Fe concentration is relatively constant compared to that of Mn; the latter shows cyclic variations; (b) the Mn concentration is distinctly antithetical to that of Fe; (c) both Co and Ni concentrations are sympathetic to the Mn concentration, and are antithetical to that of Fe; Co and Ni may therefore be associated with a Mn-rich phase, and may have been coprecipitated from seawater by the scavenging action of Mn.

It is conceivable that in the foreseeable future the necessity to recover minerals from the ocean depths will focus the first serious economic interests on the shallower, more accessible areas of the ocean. San Pablo Seamount, and similar seamounts capped with ferro-manganese deposits, may suddenly become of economic importance. Assuming a manganese pavement thickness of only one foot, the estimated tonnage of ferro-manganese ore above the 1,000 fathom contour alone would amount to over 10 million tons

(or more than 40 million tons above the 2,000 fathom contour). Apart from manganese and iron, these deposits could also be a source of nickel, cobalt, molybdenum, titanium, vanadium and other metals.

ACKNOWLEDGMENTS

We wish to thank the Chief Scientist, Dr. R. G. Gilbert, the scientific and technical staff, and the Captain, officers and crew on board the C. S. S. Hudson during cruise No. 19-67 for their enthusiastic cooperation and generous allowance of ship time. We are indebted to Dr. Gilbert for the free access and use of depth soundings and bottom photographs taken during the Hudson 19-67 cruise, and also to Dr. B. D. Loncarevic for similar material from an earlier cruise in 1966. Thanks are also due to J. J. Lynch, R. Belanger, and F. J. Cooke for their analytical and photographic assistance, and to the Metal Physics Section, Mines Branch, for the use of their electron microscope. Dr. R. J. Traill critically read the manuscript.

REFERENCES

Arrhenius, G., and Bonatti, E.
1964: Neptunism and vulcanism in the ocean; Prog. Oceanog., vol. 3, pp. 7-22.

Arrhenius, G., Mero, J., and Korkisch, J.
1964: Origin of oceanic manganese minerals; Science, vol. 144, No. 3615, pp. 170-173.

Aumento, F., and Lawrence, D. E.
1968: Photographic control of deep-sea dredging; Geol. Surv. Can., Paper 68-9.

Burns, R. G.
1965: Formation of cobalt (III) in the amorphous $FeOOH.nH_2O$ phase of manganese nodules; Nature, vol. 205, No. 4975, p. 999.

Burns, R. G., and Fuerstenau, D. W.
1966: Electron-probe determinations of inter-element relationships in manganese nodules; Am. Mineralogist, vol. 51, pp. 895-902.

Buser, W.
1959: The nature of the iron and manganese compounds in manganese nodules; Int. Oceanog. Cong., New York, N. Y., Am. Assoc. Advancement Sci. publication, pp. 962-963.

Buser, W., and Graf, P.
1955: Radiochemische Untersuchungen an Festkörpern III; Ionen- und Isotopenaustauschreaktionen an Mangandioxyden und Manganiten; Helvetica Chimica Acta., vol. 38, No. 92, pp. 810-829.

Buser, W., and Grütter, A.
1956: Über die Natur der Manganknollen; Schweiz. Mineral. Petrog. Mitt., vol. 36, No. 1, pp. 49-62.

Dieulafait, L.
1883: Le manganèse dans les eaux de mers actuelles et dans certains de leur dépôts; Compt. Rend., vol. 96, p. 718.

Goldberg, E. D., and Arrhenius, G. O. S.
1958: Chemistry of Pacific pelagic sediments; Geochimica Cosmochimica Acta, vol. 13, pp. 153-212.

Graham, J.
1959: Metabolically induced precipitation of elements from sea water; Science, vol. 129, pp. 1428-1429.

Grant, J. B.
1967: A comparison of the chemistry and mineralogy with the distribution and physical aspects of marine manganese concretions of the southern oceans; M.Sc. Thesis, Florida State University, Contribution 19, pp. 1-99.

Jenkyns, H. C.
1967: Fossil manganese nodules from Sicily; Nature, vol. 216, No. 5116, pp. 673-674.

Krauskopf, K. B.
1957: Separation of manganese from iron in sedimentary processes; Geochimica Cosmochimica Acta, vol. 12, pp. 61-84.

Ljunggren, P.
1953: Some data concerning the formation of manganiferous and ferriferous bog ores; Geol. Fören Stockholm Förh., vol. 75, pp. 277-297.

Lynn, D. C., and Bonatti, E.
1965: Mobility of manganese in diagenesis of deep-sea sediments; Marine Geol., vol. 3, pp. 457-474.

McMurdie, H. F.
1944: Microscopic and diffraction studies on dry cells and their raw materials; Trans. Electrochem. Soc., vol. 86, pp. 313-326.

Mero, J. L.
1962: Ocean-floor manganese nodules; Ec. Geol., vol. 57, pp. 747-767.

Presley, B. J., Brooks, R. R., and Kaplan, I. R.
1967: Manganese and related elements in the interstitial waters of marine sediments; Science, vol. 158, No. 3803, pp. 906-910.

Price, N. B.
1967: Some geochemical observations on manganese-iron oxide nodules from different environments; Marine Geol., vol. 5, No. 5/6, pp. 511-538.

Rona, E., Hood, O. W., Muse, L., and Buglio, B.
1962: Activation analysis of manganese and zinc in sea water; Mineral. Oceanog., vol. 7, pp. 201-206.